Supercontinuum and ultrashort-pulse generation from nonlinear Thomson and Compton scattering

K. Krajewska,[1,*] M. Twardy,[2] and J. Z. Kamiński[1]

[1]*Institute of Theoretical Physics, Faculty of Physics, University of Warsaw, Hoża 69, 00-681 Warszawa, Poland*

[2]*Faculty of Electrical Engineering, Warsaw University of Technology, Plac Politechniki 1, 00-661 Warszawa, Poland*

(Received 19 November 2013; revised manuscript received 25 February 2014; published 24 March 2014)

Nonlinear Thomson and Compton processes, in which energetic electrons collide with an intense optical pulse, are investigated in the framework of classical and quantum electrodynamics. Spectral modulations of the emitted radiation, appearing as either oscillatory or pulsating structures, are observed and explained. It is shown that both processes generate a bandwidth radiation spanning the range of a few MeV, which occurs in a small cone along the propagation direction of the colliding electrons. Most importantly, these broad bandwidth structures are temporarily coherent, which proves that Thomson and Compton processes lead to the generation of a supercontinuum. It is demonstrated that the radiation from the supercontinuum can be synthesized into zeptosecond (possibly even yoctosecond) pulses. This confirms that Thomson and Compton scattering can be used as sources of an ultrashort radiation, which opens routes to new physical domains for strong laser physics. We study properties of generated pulses arising in the classical and in the exclusively quantum regime of electron-laser-field interaction, and we attribute them to the behavior of global phases of Thomson and Compton scattering probability amplitudes.

DOI: 10.1103/PhysRevA.89.032125 PACS number(s): 12.20.Ds, 12.90.+b, 42.55.Vc, 42.65.Re

I. INTRODUCTION

Conventionally, a high-energy radiation has been produced in large-scale electron accelerators, which has resulted in a pulsed synchrotron radiation lasting for picoseconds. More compact sources of high-energy radiation have been built based on laser-wakefield electron acceleration [1]. The latter typically produce femtosecond-duration pulsed fields and, in principle, allow for conducting all-optical setup experiments [2,3]. Note that the radiation produced by either technique is very bright, tunable, nearly monoenergetic, and well collimated. These unique features make for a plethora of applications of the generated MeV radiation, including applications in natural sciences and medicine (for more details, see, for instance, [4–7]). Here, let us mention that these radiation sources are the main experimental tool for nuclear physics and astrophysics research soon to be performed at the Extreme Light Infrastructure (ELI) [8].

The key idea for generating the MeV radiation in the aforementioned setups is to allow relativistic electrons to move in an intense laser pulse, which forces them to oscillate and radiate; this is the mechanism known as *Thomson scattering* in the classical domain, with its quantum generalization known as *Compton scattering*. Consider a high-energy electron beam colliding with an intense pulse. When moving against the pulse, the electrons experience a nearly flat wave front of the pulse. Thus, it is physically justified to describe the driving field as a pulsed plane wave [9]. This approach has been used recently in connection with not only Thomson and Compton scattering [10–20], but also with other strong-field processes such as Bethe-Heitler pair creation [21], bremsstrahlung [22,23], and Mott scattering [24,25]. We will use this model in the present paper when investigating the possibility of zepto- or even yoctosecond pulse generation from Thomson and Compton processes.

It is known that Thomson and Compton scattering by a finite laser pulse lead to a spectral broadening and a modulation of emitted radiation, which is due to spectral interferences from the ramp-on and ramp-off parts of the driving pulse (cf. Refs. [11,15,17]). Note that, in contrast, a very recent classical calculation by Ghebregziabher *et al.* [26] showed that by chirping a driving pulse, the spectral broadening of high-energy radiation can be reduced. In this paper, which essentially deals with both Thomson and Compton processes, we observe additional structures of emitted radiation. We also demonstrate an appearance of a *supercontinuum* which arises from spectral broadening.

It is commonly understood that the supercontinuum is a broad bandwidth radiation generated by an interaction of a narrow bandwidth laser beam with matter. Moreover, such a spectrum should be spatially and/or temporally coherent. In this paper, we investigate coherence properties of radiation generated by nonlinear Thomson (Compton) scattering. We also show that the Thomson-originated (Compton-originated) supercontinuum allows one to produce *zeptosecond* (possibly even *yoctosecond*) pulses. Note that there are a number of papers in the literature demonstrating a possibility of ultrashort-pulse generation based on Thomson scattering [27–32]. In this paper, we demonstrate the same in the exclusively quantum regime of Compton scattering. In addition, we perform an analysis of properties of generated ultrashort pulses of radiation which arise when comparing the quantum and classical theories.

Currently, the shortest optical pulses produced in a laboratory last for 67 attoseconds [33]. Attosecond pulses are routinely produced via high-order harmonic generation (HHG) [34–36] (for recent developments, see also Ref. [37]). In order to decrease the pulse duration, significant progress has to be made to allow for the generation of ultrahigh-order harmonics.

*Katarzyna.Krajewska@fuw.edu.pl

Specifically, this can be achieved using midinfrared driving laser fields (see, e.g., Refs. [38,39]). Alternatively, x-ray radiation from free electron lasers [40] can serve as a novel tool for the synthesis of ultrashort pulses, which are expected to reach hundreds of zeptoseconds [41]. In the present paper, we show the possibility of generating subzeptosecond pulses, which is in line with previously published papers on pulse generation from Thomson radiation [27–32].

The paper is organized as follows. For the convenience of the reader, in Sec. II, we repeat the theoretical formulation of Thomson and Compton scattering as introduced in our previous papers [17,20]. In Sec. III, we present and compare the frequency spectra produced in both processes. Numerical results presented in Secs. IV and V are for such parameters for which both spectra coincide. In Sec. IV, we observe the appearance of broad bandwidth radiation, with an energy spread of a few MeV. The time dependence of this radiation is investigated in Sec. V. In Sec. VI, we demonstrate the failure of classical theory in describing properties of ultrashort pulses synthesized from emitted radiation, which is for parameters that require one to use the complete quantum theory of Compton scattering. Finally, Sec. VII summarizes our results and draws the conclusions which follow from our study.

II. THEORY

The purpose of this section is to introduce notation and to present key formulas for Compton and Thomson scattering spectra. For details of the quantum and classical formulation regarding each process, we refer the reader to Refs. [17,19,20] and [20,42–46], respectively. Since the nonlinear Compton scattering is a direct generalization of the nonlinear Thomson scattering into the quantum domain, we shall compile theory for these two processes such that the corresponding formulas are as similar as possible.

Throughout the paper, we keep $\hbar = 1$. Hence, the fine-structure constant equals $\alpha = e^2/(4\pi\varepsilon_0 c)$. We use this constant in expressions derived from classical electrodynamics as well, where it is meant to be multiplied by $\hbar$ in order to restore the physical units.

A. Basic notation

Our aim is to define the frequency-angular distribution of the electromagnetic energy that is emitted during either Compton or Thomson scattering in the form of outgoing spherical waves. Their polarization is given by a complex unit vector $\boldsymbol{\varepsilon}_{\boldsymbol{K}\sigma}$, where $\sigma = \pm$ labels two polarization degrees of freedom, and where $\boldsymbol{K}$ is the wave vector of radiation emitted in the direction $\boldsymbol{n}_{\boldsymbol{K}}$. Note that $\boldsymbol{K}$ also determines the frequency of the emitted radiation since $\omega_{\boldsymbol{K}} = c|\boldsymbol{K}|$. The wave four vector K is therefore $K = (\omega_{\boldsymbol{K}}/c)(1,\boldsymbol{n}_{\boldsymbol{K}})$, where $K^2 = 0$ and $K \cdot \varepsilon_{\boldsymbol{K}\sigma} = 0$ [we keep $\varepsilon_{\boldsymbol{K}\sigma} = (0,\boldsymbol{\varepsilon}_{\boldsymbol{K}\sigma})$ and $\varepsilon_{\boldsymbol{K}\sigma} \cdot \varepsilon^*_{\boldsymbol{K}\sigma'} = -\delta_{\sigma\sigma'}$]. We also assume that three vectors $(\boldsymbol{\varepsilon}_{\boldsymbol{K}+}, \boldsymbol{\varepsilon}_{\boldsymbol{K}-}, \boldsymbol{n}_{\boldsymbol{K}})$ form the right-handed system of mutually orthogonal unit vectors such that $\boldsymbol{\varepsilon}_{\boldsymbol{K}+} \times \boldsymbol{\varepsilon}_{\boldsymbol{K}-} = \boldsymbol{n}_{\boldsymbol{K}}$.

The laser field which drives both the nonlinear Compton and Thomson scattering is modeled as a linearly polarized, pulsed plane-wave field, with the following vector potential:

$$\boldsymbol{A}(\phi) = A_0 B \boldsymbol{\varepsilon} f(\phi). \tag{1}$$

Here, the real vector $\boldsymbol{\varepsilon}$ determines the linear polarization of the pulse, and the shape function $f(\phi)$ is defined via its derivative,

$$f'(\phi) = \begin{cases} 0, & \phi < 0, \\ \sin^2\left(\frac{\phi}{2}\right)\sin(N_{\rm osc}\phi), & 0 \le \phi \le 2\pi, \\ 0, & \phi > 2\pi, \end{cases} \tag{2}$$

where we assume that $f(0) = 0$. Above, $N_{\rm osc}$ determines the number of cycles in the pulse.

Let us further assume that the duration of the laser pulse is $T_{\rm p}$. This allows us to introduce the fundamental, $\omega = 2\pi/T_{\rm p}$, and the central frequency, $\omega_{\rm L} = N_{\rm osc}\omega$, of the laser field. Moreover, if the laser pulse propagates in a direction given by the unit vector $\boldsymbol{n}$, we can define the laser-field four vector $k = (\omega/c)(1,\boldsymbol{n})$ such that $k^2 = 0$. Hence, the phase ϕ in Eq. (1) becomes

$$\phi = k \cdot x = \omega\left(t - \frac{\boldsymbol{n}\cdot\boldsymbol{r}}{c}\right). \tag{3}$$

For our further purposes, we introduce the dimensionless and relativistically invariant parameter

$$\mu = \frac{|e|A_0}{m_e c}, \tag{4}$$

where $e = -|e|$ and m_e are the electron charge and the electron rest mass, respectively. With these notations, the laser electric and magnetic fields are equal to

$$\boldsymbol{\mathcal{E}}(\phi) = \frac{\omega m_e c \mu}{e} B \boldsymbol{\varepsilon} f'(\phi), \tag{5}$$

and

$$\boldsymbol{\mathcal{B}}(\phi) = \frac{\omega m_e \mu}{e} B(\boldsymbol{n}\times\boldsymbol{\varepsilon}) f'(\phi). \tag{6}$$

The vector potential, given by Eq. (1), and the electric component of the laser pulse, given by Eq. (5), normalized to their maximum values, are presented in Fig. 1 as functions of ϕ.

In what follows, we put $B = N_{\rm osc}$, as with this choice and for a given central laser-field frequency $\omega_{\rm L}$, the averaged intensity I of the laser pulse is independent of $N_{\rm osc}$ [21]. Specifically,

$$I = A_{\rm I}\left(\frac{\omega_{\rm L}}{m_e c^2}\right)^2 \mu^2 \langle f'^2\rangle, \tag{7}$$

where

$$\langle f'^2\rangle = \frac{1}{2\pi}\int_0^{2\pi} f'^2(\phi)\,d\phi \tag{8}$$

is equal to $3/16$ for $N_{\rm osc} > 1$, and $5/32$ for $N_{\rm osc} = 1$. If the intensity I is measured in units of W/cm^2, then $A_{\rm I} = 4.6 \times 10^{29}$.

B. Energy distributions

The theory of nonlinear Compton scattering induced by an intense laser pulse was presented in detail in Ref. [17]. It follows from there that the frequency-angular distribution of radiated Compton energy (Eqs. (51) and (52) in Ref. [17]) can be written as

$$\frac{d^3 E_{\rm C}(\boldsymbol{K},\sigma;\,\boldsymbol{p}_{\rm i},\lambda_{\rm i};\,\boldsymbol{p}_{\rm f},\lambda_{\rm f})}{d\omega_{\boldsymbol{K}} d^2\Omega_{\boldsymbol{K}}} = \alpha|\mathcal{A}_{{\rm C},\sigma}(\omega_{\boldsymbol{K}},\lambda_{\rm i},\lambda_{\rm f})|^2. \tag{9}$$

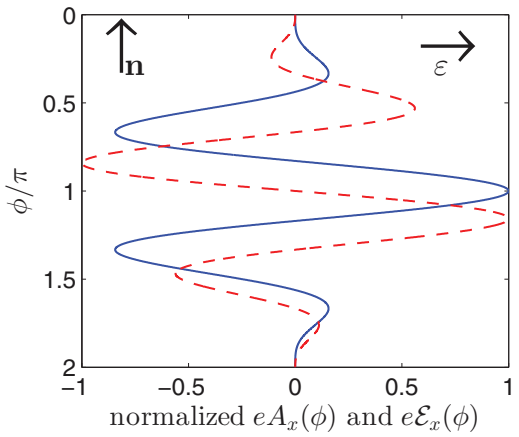

FIG. 1. (Color online) The ϕ dependence of the vector potential (solid line), given by Eq. (1), and the electric field (dashed line), given by Eq. (5), multiplied by the electron charge and normalized to their maximum values are plotted for $N_{\rm osc} = 3$. The pulse propagates in the z direction, $\boldsymbol{n} = \boldsymbol{e}_z$, and the linear polarization vector points into the x direction, $\boldsymbol{\varepsilon} = \boldsymbol{e}_x$. The vector potential curve possesses the mirror symmetry with respect to the horizontal line $\phi/\pi = 1$, and the electric-field line exhibits the axial symmetry with respect to the point (0,1).

The above formula relates to the electromagnetic energy emitted (as spherical outgoing waves) if the initial electron has momentum $\boldsymbol{p}_{\rm i}$ and spin polarization $\lambda_{\rm i}$, whereas the final electron has the spin polarization $\lambda_{\rm f}$ and its momentum is determined by the momentum conservation equations (cf. Eqs. (47) in Ref. [17]). We shall call the complex function $\mathcal{A}_{{\rm C},\sigma}(\omega_{\boldsymbol{K}},\lambda_{\rm i},\lambda_{\rm f})$ the Compton amplitude; it is worth noting that it also depends on the remaining parameters of the Compton scattering, but we display explicitly only those which are essential for our further discussion. If one is not interested in the dependence of emitted radiation on the electron spin degrees of freedom, then the distribution above has to be summed over the final and averaged over the initial spin polarizations. This leads to

$$\frac{d^3E_{\rm C}(\boldsymbol{K},\sigma)}{d\omega_{\boldsymbol{K}}d^2\Omega_{\boldsymbol{K}}} = \frac{\alpha}{2}\sum_{\lambda_{\rm i},\lambda_{\rm f}=\pm}|\mathcal{A}_{{\rm C},\sigma}(\omega_{\boldsymbol{K}},\lambda_{\rm i},\lambda_{\rm f})|^2, \qquad (10)$$

where all irrelevant electron degrees of freedom are hidden.

The complete theory of nonlinear Thomson scattering is presented in Jackson's textbook [42] (see, also, Ref. [20]). The relevant frequency-angular distribution of energy emitted during this process can be expressed as

$$\frac{d^3E_{\rm Th}(\boldsymbol{K},\sigma)}{d\omega_{\boldsymbol{K}}d^2\Omega_{\boldsymbol{K}}} = \alpha|\mathcal{A}_{{\rm Th},\sigma}(\omega_{\boldsymbol{K}})|^2, \qquad (11)$$

and it should be compared with Eqs. (9) or (10) for Compton scattering. In analogy with the Compton theory, the complex function $\mathcal{A}_{{\rm Th},\sigma}(\omega_{\boldsymbol{K}})$ will be called here the Thomson amplitude. As shown in Ref. [20], its explicit form can be represented as an integral,

$$\mathcal{A}_{{\rm Th},\sigma}(\omega_{\boldsymbol{K}}) = \frac{1}{2\pi}\int_0^{2\pi} d\phi\,\Upsilon_\sigma(\phi)\exp[i\omega_{\boldsymbol{K}}\ell(\phi)/c], \qquad (12)$$

where

$$\ell(\phi) = c\frac{\phi}{\omega} + (\boldsymbol{n}-\boldsymbol{n}_{\boldsymbol{K}})\cdot\boldsymbol{r}(\phi), \qquad (13)$$

$$\Upsilon_\sigma(\phi) = \boldsymbol{\varepsilon}^*_{\boldsymbol{K}\sigma}\cdot\frac{\boldsymbol{n}_{\boldsymbol{K}}\times\{[\boldsymbol{n}_{\boldsymbol{K}}-\boldsymbol{\beta}(\phi)]\times\boldsymbol{\beta}'(\phi)\}}{[1-\boldsymbol{n}_{\boldsymbol{K}}\cdot\boldsymbol{\beta}(\phi)]^2}, \qquad (14)$$

and where the electron position $\boldsymbol{r}(\phi)$ and reduced velocity $\boldsymbol{\beta}(\phi)$ fulfill the system of ordinary differential equations,

$$\frac{d\boldsymbol{r}(\phi)}{d\phi} = \frac{c}{\omega}\frac{\boldsymbol{\beta}(\phi)}{1-\boldsymbol{n}\cdot\boldsymbol{\beta}(\phi)},$$

$$\frac{d\boldsymbol{\beta}(\phi)}{d\phi} = \mu\frac{\sqrt{1-\boldsymbol{\beta}^2(\phi)}}{1-\boldsymbol{n}\cdot\boldsymbol{\beta}(\phi)}[\{\boldsymbol{\varepsilon}-\boldsymbol{\beta}(\phi)[\boldsymbol{\beta}(\phi)\cdot\boldsymbol{\varepsilon}]+\boldsymbol{\beta}(\phi) \times(\boldsymbol{n}\times\boldsymbol{\varepsilon})\}f'(\phi)]. \qquad (15)$$

Let us recall that these equations can be derived from the Newton-Lorentz relativistic equations, with time t which relates to the phase ϕ by Eq. (3).

III. SCATTERING AMPLITUDES

Let us start by comparing the quantum Compton process with its classical approximation which is the Thomson process, in which both are driven by a three-cycle laser pulse ($N_{\rm osc} = 3$) with the electric and magnetic fields defined by the shape function (2) (see, also, Fig. 1). We choose the reference frame such that the pulse propagates in the z direction, $\boldsymbol{n} = \boldsymbol{e}_z$, and its linear polarization vector is $\boldsymbol{\varepsilon} = \boldsymbol{e}_x$, whereas the initial electron velocity vanishes, i.e., initially electrons are at rest. In Figs. 2 and 3, we compare the quantum and classical theories for the same pulse configuration but for two different directions of observation of scattered radiation. For both directions of emission, we see that the Compton spectrum is compressed in comparison with the Thomson spectrum. As discussed

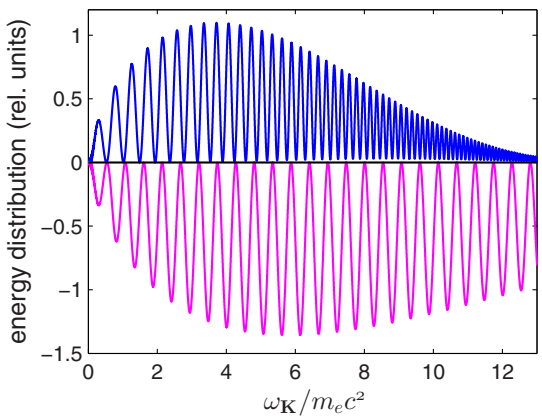

FIG. 2. (Color online) Energy spectra for Compton scattering (upper panel), given by Eq. (10), and for Thomson scattering (lower panel, reflected with respect to the horizontal black line), given by Eq. (11). The laser-field parameters are such that $\mu = 10$, $N_{\rm osc} = 3$, $\omega_{\rm L} = 0.03m_ec^2$, and the scattered radiation is linearly polarized in the scattering plane, i.e., in the (xz) plane. The direction of scattered radiation is given by the polar and azimuthal angles, $\theta_{\boldsymbol{K}} = 0.1\pi$ and $\varphi_{\boldsymbol{K}} = \pi$, respectively. These parameters are specified in the rest frame of incident electrons.

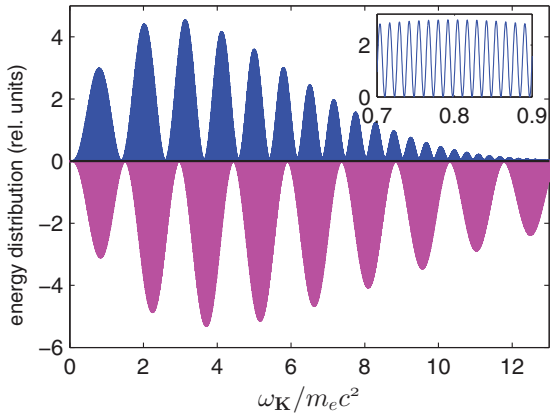

FIG. 3. (Color online) The same as in Fig. 2 but for the polar and azimuthal angles, $\theta_{\boldsymbol{K}} = 0.1\pi$ and $\varphi_{\boldsymbol{K}} = 0$, respectively. In the inset, we present the enlarged portion of the Compton distribution with regular oscillations of the energy spectrum.

in Ref. [20], such a nonlinear compression of the Compton distribution (note that the larger the frequency, the more compressed the spectrum is) indicates the quantum nature of Compton scattering. If for the Thomson scattering we denote the frequency as $\omega_{\boldsymbol{K}}^{\mathrm{Th}}$ and scale it to $\omega_{\boldsymbol{K}}$ according to the rules

$$\omega_{\mathrm{cut}} = c\frac{n\cdot p_{\mathrm{i}}}{n\cdot n_{\boldsymbol{K}}} = \frac{m_e c^2}{1-\cos\theta_{\boldsymbol{K}}} \approx 20.4 m_e c^2, \tag{16}$$

and

$$\omega_{\boldsymbol{K}}^{\mathrm{Th}} - \omega_{\boldsymbol{K}} = \frac{\omega_{\boldsymbol{K}}^{\mathrm{Th}}\omega_{\boldsymbol{K}}}{\omega_{\mathrm{cut}}}, \tag{17}$$

then both spectra become similar to each other. Namely, they have maxima and minima for the same frequencies, but their absolute values can differ. In Eq. (16), we have introduced the cutoff frequency ω_{cut}, which defines the maximum frequency for the Compton scattering. It appears that both quantum and classical approaches give the same results for the aforementioned absolute values, provided that $\omega_{\boldsymbol{K}} \ll \omega_{\mathrm{cut}}$. Moreover, as it follows from the discussion presented in Ref. [20], even for frequencies close to the cutoff, both distributions remain similar when helicities of the initial and final electron states are the same.

However, when comparing Figs. 2 and 3, we observe that the presented distributions look qualitatively different. While for the first case we observe slowly pulsating spectra, for the second case the spectra are modulated and exhibit very rapid oscillations. It is well known that the reason for the oscillatory behavior of energy distributions is the interference of scattered radiation, but this does not explain the qualitative difference between these two cases. It could be attributed, for instance, to the right-left asymmetry of the laser-field potential (Fig. 1), as it has been discussed for the case of electron-positron pair creation [47]. In order to analyze this problem in detail, we found it very difficult (if not impossible) to dwell on the Compton theory, due to its complicated character. However, such a discussion can be based on the Thomson theory, which we present below. We stress that electron-laser-field scattering with emission of extra photons is actually described by the

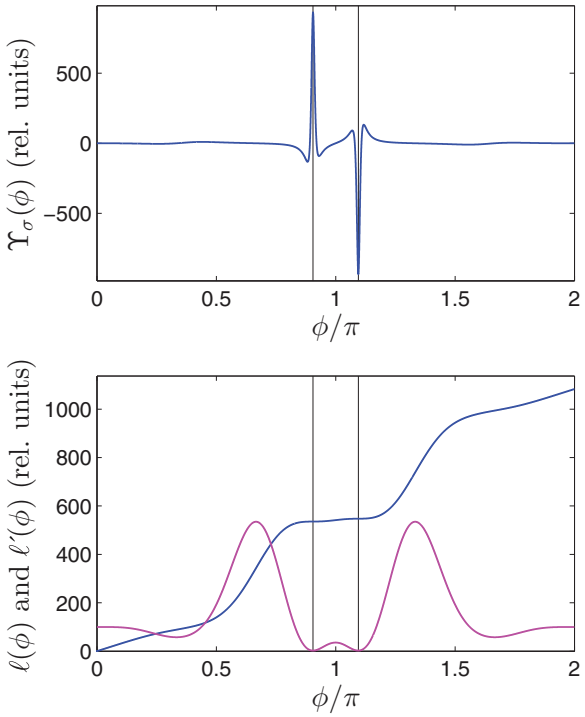

FIG. 4. (Color online) The functions $\Upsilon_\sigma(\phi)$ (upper frame), given by Eq. (14), and $\ell(\phi)$ and its derivative $\ell'(\phi)$ (lower frame), given by Eq. (13), for the scattering parameters of Fig. 2. Two thin vertical lines mark the positions of the dominant extrema of $\Upsilon_\sigma(\phi)$, for $\phi_1 \approx 0.9\pi$ and $\phi_2 = 2\pi - \phi_1$. In the lower frame, the blue (dark; monotonously increasing) line represents the $\ell(\phi)$ function, whereas the magenta (gray; exhibiting extrema) line represents the $\ell'(\phi)$ function.

Compton scattering, and that Thomson scattering can *only* be treated as its approximation. Therefore, the classical theory can be used to interpret the results whenever (within the range of its applicability) it is difficult to provide a reasonable physical interpretation based on the more complete quantum theory.

Let us consider the first case, shown in Fig. 2, and draw the functions $\Upsilon_\sigma(\phi)$, $\ell(\phi)$, and its derivative $\ell'(\phi)$, as presented in Fig. 4. We observe here two main extrema of $\Upsilon_\sigma(\phi)$ for $\phi_1 \approx 0.9\pi$ and $\phi_2 = 2\pi - \phi_1$, the position of which coincide with two global minima of $\ell'(\phi)$. Since

$$\ell'(\phi) = \frac{c}{\omega}\frac{1-\boldsymbol{n}_{\boldsymbol{K}}\cdot\boldsymbol{\beta}(\phi)}{1-\boldsymbol{n}\cdot\boldsymbol{\beta}(\phi)} > 0, \tag{18}$$

we attribute these extrema to the minimum value of the denominator in Eq. (14). Moreover, the function $\Upsilon_\sigma(\phi)$ exhibits a very sharp maximum and minimum, therefore, the Thomson amplitude, given by Eq. (12), can be approximated by two terms,

$$\mathcal{A}_{\mathrm{Th},\sigma}(\omega_{\boldsymbol{K}}) \approx A(e^{i\omega_{\boldsymbol{K}}\ell(\phi_1)/c} - e^{i\omega_{\boldsymbol{K}}\ell(\phi_2)/c}). \tag{19}$$

Here, A is roughly equal to the area under the peak. More precisely, A is a slowly varying function of $\omega_{\boldsymbol{K}}$ which can be calculated by applying a better approximation, for instance, the saddle-point method for sufficiently large $\omega_{\boldsymbol{K}}$. However, for the purpose of our further discussion, it is sufficient to consider A as a constant.

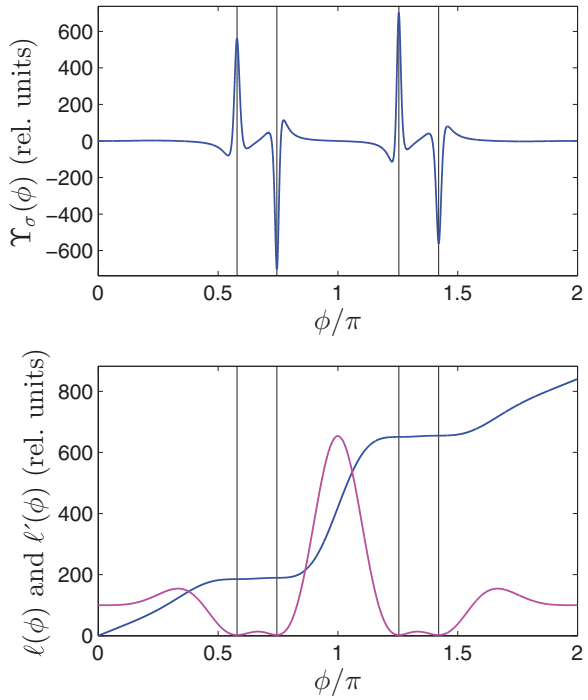

FIG. 5. (Color online) The same as in Fig. 4 but for the scattering parameters of Fig. 3. Four thin vertical lines indicate positions of the dominant extrema of $\Upsilon_\sigma(\phi)$, for $\phi_1 \approx 0.58\pi$, $\phi_2 = 0.75\pi$, $\phi_3 = 2\pi - \phi_1$, and $\phi_4 = 2\pi - \phi_2$. The analysis of the numerical data shows that $\ell(\phi_1) = \tau_0 - \tau_{\rm big} - \tau_{\rm small}$, $\ell(\phi_2) = \tau_0 - \tau_{\rm big} + \tau_{\rm small}$, $\ell(\phi_3) = \tau_0 + \tau_{\rm big} - \tau_{\rm small}$, and $\ell(\phi_4) = \tau_0 + \tau_{\rm big} + \tau_{\rm small}$, with $\tau_0 \approx 420/m_e c$, $\tau_{\rm big} \approx 233/m_e c$, and $\tau_{\rm small} \approx 2.14/m_e c$.

It follows from the numerical data that

$$\ell(\phi_1) = \tau_0 - \tau_{\rm small} \quad \text{and} \quad \ell(\phi_2) = \tau_0 + \tau_{\rm small}, \tag{20}$$

with $\tau_0 \approx 541.5/m_e c$ and $\tau_{\rm small} \approx 5.9/m_e c$. The modulus squared of the pulsating part of Thomson amplitude is therefore proportional to

$$|\mathcal{A}_{{\rm Th},\sigma}(\omega_{\boldsymbol{K}})|^2 \propto \sin^2\left(5.9\frac{\omega_{\boldsymbol{K}}}{m_e c^2}\right). \tag{21}$$

This means that two consecutive minima in the Thomson distribution are separated by $\Delta\omega_{\boldsymbol{K}}/m_e c^2 \approx \pi/5.9 \approx 0.53$, which agrees very well with the data presented in Fig. 2.

A similar interpretation can be attributed to the modulated and rapidly oscillating energy distributions presented in Fig. 3. In this case, we have four main extrema (cf. Fig. 5). Although the outer extrema are smaller in magnitude than the inner ones, they are also more spread out. Therefore, in the first approximation, we can assume that the related areas (under the maxima and above the minima) are equal to each other. This leads to the approximate form for the Thomson amplitude,

$$\mathcal{A}_{{\rm Th},\sigma}(\omega_{\boldsymbol{K}}) \approx A\sum_{s=1}^{4}(-1)^{s+1}e^{i\omega_{\boldsymbol{K}}\ell(\phi_s)/c}. \tag{22}$$

Hence,

$$|\mathcal{A}_{{\rm Th},\sigma}(\omega_{\boldsymbol{K}})|^2 \propto \sin^2\left(2.14\frac{\omega_{\boldsymbol{K}}}{m_e c^2}\right)\sin^2\left(233\frac{\omega_{\boldsymbol{K}}}{m_e c^2}\right), \tag{23}$$

which again agrees very well with the data presented in Fig. 3. In this case, the consecutive minima of fast oscillations are separated by $\Delta\omega_{\boldsymbol{K}}/m_e c^2 \approx \pi/233 \approx 0.013$, whereas for the modulation, we obtain $\delta\omega_{\boldsymbol{K}}/m_e c^2 \approx \pi/2.14 \approx 1.46$. In other words, there are more than 100 oscillations within a single modulation.

IV. GENERATION OF SUPERCONTINUUM

Since its demonstration in the early 1970s [48], the supercontinuum generation has been the focus of significant research activity. It has attracted much attention owing to its enormous spectral broadening (for instance, it is possible to obtain a white-light spectrum covering the entire visible range from 400 to 700 nm), which have many useful applications in telecommunication [49], frequency metrology [50], optical coherence tomography [51], and device characterization [52]. It has to be mentioned, however, that the supercontinuum generation in photonics is, in general, a complex physical phenomenon involving many nonlinear optical effects such as self-phase modulation, cross-phase modulation, four-wave mixing, and stimulated Raman scattering [53]. It seems to be simpler to analyze the generation of a broadband spectrum of radiation by the Thomson and Compton scattering.

A closer look at Fig. 2 suggests that the Thomson (or Compton) process could be used for the generation of a supercontinuum with the bandwidth of a few keV and with a small change of its intensity. It is shown, for instance, by the first pulsation in the energy distribution, the width of which is around 200 keV in the reference frame of electrons. In order to further investigate such a possibility, below we study the nonlinear Thomson scattering in the laboratory frame. Since we are going to consider the spectrum of frequencies much smaller than the cutoff frequency (16), the Thomson and Compton theories give practically the same results. The former, however, can be numerically treated much faster.

In the analysis of Thomson and Compton processes in the laboratory frame, we have to account for the fact that the initial energy of electrons has to be large, as compared to $m_e c^2$, in order to generate sufficiently intense pulses of scattered radiation. Moreover, the laser pulse central frequency $\omega_{\rm L}$ is much smaller than $m_e c^2$. This means that the majority of the generated radiation is emitted in a very sharp cone. In particular, for a head-on collision of the laser and electron beams, when electrons are moving in the direction opposite to the z axis, the radiation is scattered for $\theta_{\boldsymbol{K}}$ very close to π. In this case, the parametrization of all possible directions of emission by two spherical angles $\theta_{\boldsymbol{K}}$ and $\varphi_{\boldsymbol{K}}$ is not convenient, as it will follow shortly. It is better to consider another system of Cartesian coordinates (x',y',z') such that (cf. Refs. [17,54])

$$(x',y',z') = (z,x,y). \tag{24}$$

If, in the new system of coordinates, we denote the polar angle by $\Phi_{\boldsymbol{K}}$ $(0 \le \Phi_{\boldsymbol{K}} \le \pi)$ and the azimuthal angle by $\Theta_{\boldsymbol{K}}$ $(0 \le \Theta_{\boldsymbol{K}} < 2\pi)$, then they can be related to the original polar and azimuthal angles $\theta_{\boldsymbol{K}}$ and $\varphi_{\boldsymbol{K}}$ by the equations

$$\Phi_{\boldsymbol{K}} = \arccos(\sin\theta_{\boldsymbol{K}}\sin\varphi_{\boldsymbol{K}}) \tag{25}$$

and

$$\tan\Theta_{\boldsymbol{K}} = \tan\theta_{\boldsymbol{K}}\cos\varphi_{\boldsymbol{K}}. \tag{26}$$

In addition, the scattering plane (xz), which before was defined by two conditions, $\varphi_{\boldsymbol{K}} = 0$ and $\varphi_{\boldsymbol{K}} = \pi$, now is defined by the single condition $\Phi_{\boldsymbol{K}} = \pi/2$. The discontinuous change of angles $(\theta_{\boldsymbol{K}},\varphi_{\boldsymbol{K}}) = (\pi-\varepsilon,0) \to (\pi-\varepsilon,\pi)$, $\varepsilon \ll 1$, which corresponds to the continuous change of directions near the south pole of the unit sphere, now is described by the continuous change of angles $(\Phi_{\boldsymbol{K}},\Theta_{\boldsymbol{K}}) = (\pi/2,\pi-\varepsilon) \to (\pi/2,\pi+\varepsilon)$. It is, therefore, more convenient to use the angles $(\Phi_{\boldsymbol{K}},\Theta_{\boldsymbol{K}})$ in our analysis. Since the infinitesimal solid angle becomes

$$d^2\Omega_{\boldsymbol{K}} = \sin\Phi_{\boldsymbol{K}} d\Phi_{\boldsymbol{K}} d\Theta_{\boldsymbol{K}}, \tag{27}$$

we can define the partially integrated energy spectrum of emitted radiation for the Thomson process,

$$\frac{d^2E_{\rm Th}(\boldsymbol{K},\sigma)}{\sin\Phi_{\boldsymbol{K}} d\omega_{\boldsymbol{K}} d\Phi_{\boldsymbol{K}}} = \int_0^{2\pi} d\Theta_{\boldsymbol{K}} \frac{d^3E_{\rm Th}(\boldsymbol{K},\sigma)}{d\omega_{\boldsymbol{K}} d^2\Omega_{\boldsymbol{K}}}, \tag{28}$$

and similarly for the Compton process. Next, we can define the angular distribution,

$$\frac{d^2E_{\rm Th}(\boldsymbol{n}_{\boldsymbol{K}},\sigma)}{d^2\Omega_{\boldsymbol{K}}} = \int_0^{\omega_{\rm max}} d\omega_{\boldsymbol{K}} \frac{d^3E_{\rm Th}(\boldsymbol{K},\sigma)}{d\omega_{\boldsymbol{K}} d^2\Omega_{\boldsymbol{K}}}, \tag{29}$$

where we have introduced the maximum frequency, $\omega_{\rm max}$. This frequency is infinite for Thomson scattering, but it is equal to the cutoff frequency (16) for Compton scattering [20], independent of the incident pulse duration.

In Fig. 6, we present the color map of energy distributions for the Thomson process as a function of frequency and emission angle in the scattering plane, i.e., for $\Phi_{\boldsymbol{K}} = \pi/2$. It clearly demonstrates that, for frequencies around $8m_ec^2$ (4 MeV) and $16m_ec^2$ (8 MeV), intense and very broad (of the order of 2 MeV) candidates for the supercontinuum

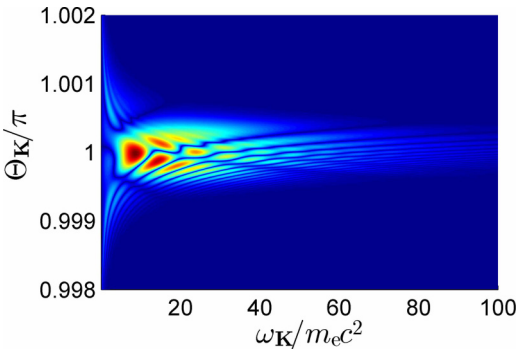

FIG. 6. (Color online) Color map of the energy distribution for the Thomson process, given by Eq. (11). We assume a three-cycle driving pulse, linearly polarized in the x direction [for the shape function of the electric-field component, see Eq. (2)], counterpropagating an electron beam. The pulse central frequency in the laboratory frame equals $\omega_{\rm L} = 1.548$ eV $\approx 3\times10^{-6}m_ec^2$ and its averaged intensity is determined by $\mu = 1$ [Eq. (7)]. Electrons move in the opposite z direction, with momentum $|\boldsymbol{p}_{\rm i}| = 1000m_ec$ and the scattering process occurs in the plane $\Phi_{\boldsymbol{K}} = \pi/2$ [see Eqs. (25) and (26) for the definitions of angles $\Phi_{\boldsymbol{K}}$ and $\Theta_{\boldsymbol{K}}$]. The emitted radiation is linearly polarized in the (xz) plane [or, equivalently, in the $(x'y')$ plane].

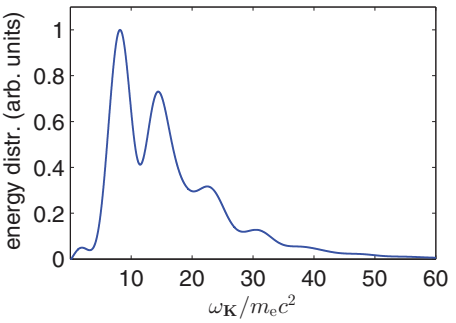

FIG. 7. (Color online) The energy differential distribution of emitted radiation integrated over $\Theta_{\boldsymbol{K}}$, given by Eq. (28), and normalized to its maximum value, for the same geometry and parameters as in Fig. 6.

are created. Note also that for the considered electron- and laser-beam parameters, the radiation is scattered within a very narrow cone. Although we have presented results for a particular $\Phi_{\boldsymbol{K}}$, the pattern also preserves its structure for the polar angle $\Phi_{\boldsymbol{K}}$ close to $\pi/2$. Figure 7 shows the partially integrated energy distribution, given by Eq. (28), for $\Phi_{\boldsymbol{K}} = \pi/2$ with two broad peaks. In order to call these structures the supercontinuum, we have to investigate their coherent properties. For Compton processes, this problem has been partially discussed in [55]. We have shown there that the phase of the Compton probability amplitude is not random and it linearly increases with $\omega_{\boldsymbol{K}}$ in the frequency intervals sufficiently wide in order to cover at least a few interference peaks in the energy distribution. We have checked that the same occurs for Thomson scattering. This suggests that a synthesis of frequencies from the supercontinuum indeed can lead to the generation of very short pulses of radiation.

V. TEMPORAL POWER DISTRIBUTIONS

In the previous section, we have demonstrated the possibility of the generation of a very broad spectrum of radiation, with the bandwidth of a few MeV. In order to show the coherent properties of this spectrum, one has to investigate the time dependence of scattered radiation and check if it can be used for the synthesis of very short pulses. This is the case, for instance, of HHG in gases [56], plasmas [57], and crystals [58], which are routinely used for the synthesis of attosecond pulses (for a review concerning HHG, see, also, Ref. [37]). Thus, we need to relate the frequency-angular distributions of the energy of generated radiation to the temporal power distribution of the emitted radiation. For simplicity, we shall do it now for the classical theory.

By analyzing the Liénard-Wiechert potentials [42,43], it is straightforward to relate the Thomson amplitude $\mathcal{A}_{{\rm Th},\sigma}(\omega_{\boldsymbol{K}})$ to the electric field of the scattered radiation. Indeed, the Fourier transform of the electric field of polarization $\boldsymbol{\varepsilon}_{\boldsymbol{K}\sigma}$, in the far radiation zone, has the form of the outgoing spherical wave

$$\tilde{\mathcal{E}}_\sigma(\omega_{\boldsymbol{K}}) = \frac{e^{i|\boldsymbol{K}|R}}{R}\frac{e}{4\pi\varepsilon_0 c}2\pi\mathcal{A}_{{\rm Th},\sigma}(\omega_{\boldsymbol{K}}), \tag{30}$$

with its space-time form,

$$\mathcal{E}_\sigma\left(t-\frac{R}{c}\right)=\int_{-\infty}^{\infty}\frac{d\omega}{2\pi}e^{-i\omega t}\tilde{\mathcal{E}}_\sigma(\omega). \tag{31}$$

In this notation, we show explicitly the time dependence of the electric field, whereas the decay $1/R$, being less important for our further discussion, is hidden. To make the notation shorter, we introduce the retarded phase

$$\phi_{\rm r}=\omega_0\left(t-\frac{R}{c}\right), \tag{32}$$

and rewrite Eq. (31) as

$$\mathcal{E}_\sigma(\phi_{\rm r})=\frac{e}{4\pi\varepsilon_0 cR}\tilde{\mathcal{A}}_{{\rm Th},\sigma}(\phi_{\rm r}), \tag{33}$$

where

$$\tilde{\mathcal{A}}_{{\rm Th},\sigma}(\phi_{\rm r})=\int_{-\infty}^{\infty}d\omega\mathcal{A}_{{\rm Th},\sigma}(\omega)e^{-i\omega\phi_{\rm r}/\omega_0}. \tag{34}$$

In the definition of $\phi_{\rm r}$, we have introduced an arbitrary frequency ω_0. We shall discuss below which value for this parameter should be chosen.

Since the electric field is real, we have $\mathcal{A}_{{\rm Th},\sigma}(-\omega)=\mathcal{A}^*_{{\rm Th},\sigma}(\omega)$. Defining

$$\tilde{\mathcal{A}}^{(+)}_{{\rm Th},\sigma}(\phi_{\rm r})=\int_{0}^{\infty}d\omega\mathcal{A}_{{\rm Th},\sigma}(\omega)e^{-i\omega\phi_{\rm r}/\omega_0}, \tag{35}$$

we find that

$$\mathcal{E}_\sigma(\phi_{\rm r})=\frac{e}{4\pi\varepsilon_0 cR}2{\rm Re}\tilde{\mathcal{A}}^{(+)}_{{\rm Th},\sigma}(\phi_{\rm r}), \tag{36}$$

where the symbol Re means the real value. Applying the Poynting theorem of classical electrodynamics [42,43], we find that the total energy of scattered radiation transmitted through an infinitesimal surface $R^2d\Omega_{\boldsymbol{K}}$ equals

$$d^2E_{{\rm Th},\sigma}=d^2\Omega_{\boldsymbol{K}}\frac{\alpha}{\pi}\int_{-\infty}^{\infty}dt[{\rm Re}\tilde{\mathcal{A}}^{(+)}_{{\rm Th},\sigma}(\phi_{\rm r})]^2. \tag{37}$$

This allows us to define the angular distribution of temporal power of emitted radiation,

$$\frac{d^2P_{{\rm Th},\sigma}(\phi_{\rm r})}{d^2\Omega_{\boldsymbol{K}}}=\frac{\alpha}{\pi}[{\rm Re}\tilde{\mathcal{A}}^{(+)}_{{\rm Th},\sigma}(\phi_{\rm r})]^2. \tag{38}$$

For the Compton scattering, the corresponding temporal power distribution looks similar, except that the Compton amplitude, $\mathcal{A}_{{\rm C},\sigma}(\omega_{\boldsymbol{K}};\lambda_{\rm i},\lambda_{\rm f})$, depends also on the electron spin degrees of freedom.

Similarly to the integrated energy distributions, given by Eqs. (28) and (29), we can define the integrated power distribution of Thomson radiation,

$$\frac{dP_{{\rm Th},\sigma}(\phi_{\rm r})}{\sin\Phi_{\boldsymbol{K}}d\Phi_{\boldsymbol{K}}}=\int_0^{2\pi}d\Theta_{\boldsymbol{K}}\frac{d^2P_{{\rm Th},\sigma}(\phi_{\rm r})}{d^2\Omega_{\boldsymbol{K}}}, \tag{39}$$

and its angular distribution,

$$\frac{d^2E_{\rm Th}(\boldsymbol{n}_{\boldsymbol{K}},\sigma)}{d^2\Omega_{\boldsymbol{K}}}=\frac{1}{\omega_0}\int_0^{\phi_{\max}}d\phi_{\rm r}\frac{d^2P_{{\rm Th},\sigma}(\phi_{\rm r})}{d^2\Omega_{\boldsymbol{K}}}. \tag{40}$$

Here, we have introduced the maximum value $\phi_{\max}$ for the retarded phase $\phi_{\rm r}$, which has the purely numerical origin and it is closely related to the parameter ω_0 used in Eq. (32). Indeed, numerically, the Thomson and Compton amplitudes are calculated for some discrete values $\omega_{\boldsymbol{K}}$; in our case, we choose the equally spaced values with a step $\Delta\omega_{\boldsymbol{K}}$. For instance, in our calculations presented in Fig. 6, we have chosen 10^4 points in the frequency interval $[0,100m_ec^2]$, which means that $\Delta\omega_{\boldsymbol{K}}=0.01m_ec^2$. The Fourier transform of the amplitudes [for the Thomson scattering, see Eq. (35)] is then calculated using the trapezoid algorithm for the integration. This means that we observe artificial revivals of $\tilde{\mathcal{A}}^{(+)}_{{\rm Th},\sigma}(\phi_{\rm r})$, separated by

$$\Delta\phi_{\rm r}=2\pi\frac{\omega_0}{\Delta\omega_{\boldsymbol{K}}}. \tag{41}$$

Therefore, in order to make them well separated from the real contribution, we have to choose ω_0 much larger than $\Delta\omega_{\boldsymbol{K}}$. In the numerical analysis presented above, we have put $\omega_0=m_ec^2$, which means that the closest artificial revivals appear for $\phi_{\rm r}\approx\pm200\pi$, and by increasing ω_0, we also increase their distance. This also puts the bound on $\phi_{\max}$; the maximum phase $\phi_{\max}$ should be large but cannot exceed $\Delta\phi_{\rm r}$. Lastly, it is important to note that two integrated distributions, given by Eqs. (29) and (40), represent the same quantity and should give the same results.

In Fig. 8, we present the energy distribution of radiation emitted in the direction $(\theta_{\boldsymbol{K}},\varphi_{\boldsymbol{K}})=(0.99999\pi,\pi)$ or, equivalently, for $(\Phi_{\boldsymbol{K}},\Theta_{\boldsymbol{K}})=(\pi/2,1.00001\pi)$. The distribution shows typical interference structures. The synthesis of this

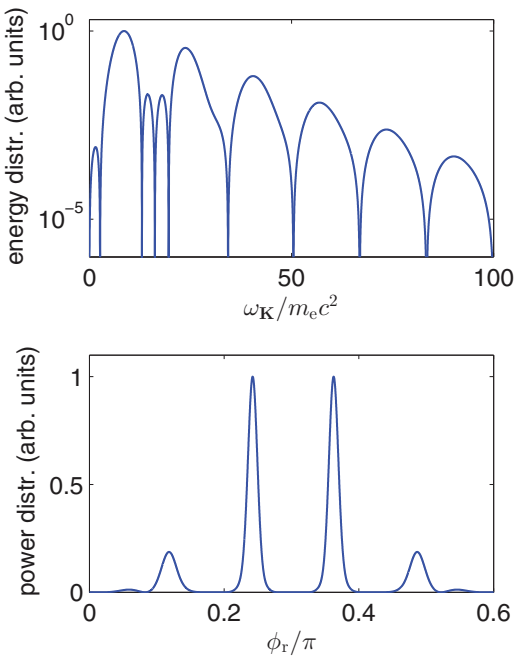

FIG. 8. (Color online) The energy distribution (upper panel), given by Eq. (11), and the power distribution (lower panel), given by Eq. (38), for the Thomson scattering. The geometry and the laser- and electron-beam parameters are the same as in Fig. 6, except that the results are presented for $\Theta_{\boldsymbol{K}}=1.00001\pi$ [or, equivalently, $(\theta_{\boldsymbol{K}},\varphi_{\boldsymbol{K}})=(0.99999\pi,\pi)$]. The emitted radiation is polarized in the (xz) plane and the distributions are normalized to their maximum values. For the power distribution, we put $\omega_0=m_ec^2$, while the upper limit of the frequency integration in (35) we set to $100m_ec^2$.

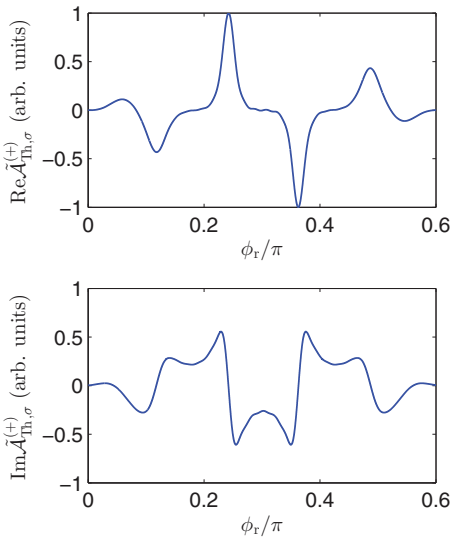

FIG. 9. (Color online) The real (upper panel) and imaginary (lower panel) parts of the Fourier transform of the Thomson amplitude, given by Eq. (35), normalized to the maximum value of $\mathrm{Re}\tilde{\mathcal{A}}^{(+)}_{\mathrm{Th},\sigma}$. The plots are for the parameters from Fig. 8. The real part of the Fourier transform is proportional to the electric field of the emitted radiation.

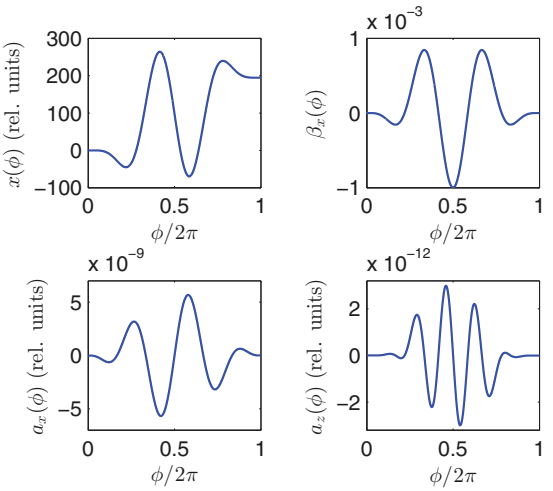

FIG. 10. (Color online) The electron classical trajectory for the parameters considered in Fig. 8. In the upper row, the projections of the position and reduced velocity vectors on the laser-field polarization axis are presented as functions of the phase ϕ, given by Eq. (3). In the lower row, two nonvanishing projections of the acceleration vector $\boldsymbol{a}(\phi)$ on the laser-field polarization and propagation vectors, $\boldsymbol{\varepsilon}$ and $\boldsymbol{k}$, are shown. While the reduced velocity $\boldsymbol{\beta}(\phi)$ is dimensionless, the quantities $\boldsymbol{r}(\phi)$ and $\boldsymbol{a}(\phi)$ are in the relativistic units of length, $\lambda\!\!\!^{-}_{\mathrm{C}} \approx 3.86 \times 10^{-13}$ m, and acceleration, $\lambda\!\!\!^{-}_{\mathrm{C}}(m_e c^2)^2 \approx 2.3 \times 10^{29}$ m/s^2.

frequency pattern to the time domain exhibits two main peaks together with two small side lobes. The width of these peaks are of the order of $\delta\phi_r \approx 0.1$, which means that they last for roughly $\delta t \approx 0.1/m_e c^2 = 0.1 t_C$, where t_C is the Compton time,

$$t_C = \frac{\lambda\!\!\!^{-}_{\mathrm{C}}}{c} = \frac{1}{m_e c^2} \approx 1.3 \times 10^{-21}\ \mathrm{s}. \tag{42}$$

This time is many orders of magnitude smaller than the interaction time of electrons with the laser pulse, which for the considered energy of electrons is a bit larger than $T_p/2$.

This clearly proves the coherent properties of the high-frequency supercontinuum generated in the laser-induced nonlinear Thomson (Compton) scattering. This supercontinuum can be synthesized to very short (zepto- or even yoctosecond) pulses. Let us also remark that within such a pulse, the electric field does not oscillate, as it is presented in Fig. 9. This means that the emitted radiation is generated practically in the form of a "one-cycle" pulse, or even well separated into two "half-cycle" pulses. This is, of course, the consequence of the three-cycle pulse used as a driving force.

For completeness of our discussion, in Fig. 10 we plot the components of position, reduced velocity, and acceleration vectors of the electron classical trajectory for the physical parameters and geometry considered in Fig. 8. For this geometry, the classical dynamics occurs in the scattering plane. Moreover, since the energy of the electron beam is much larger than the ponderomotive energy of the laser pulse, the z components of the position and reduced velocity vectors are only marginally modified by the laser pulse, and so they are not presented in the figure. As expected, the x component of the reduced velocity, $\beta_x(\phi)$, follows the temporal dependence of the vector potential (solid line in Fig. 1), whereas the x component of the acceleration vector, $a_x(\phi)$, shows similarities with the temporal behavior of the electric field (dashed line in Fig. 1). The latter determines the shape of the real part of the Fourier transform of the Thomson amplitude, given by Eq. (35) and shown in Fig. 9, as well as the temporal dependence of the power distribution, shown in Fig. 8. Let us remark that for the considered laser- and electron-beam parameters, we observe a rather smooth dependence of the position, reduced velocity, and acceleration on the phase ϕ. For larger intensities, this dependence starts to exhibit sharp features. This will lead to more complicated structures in the differential energy distribution of emitted radiation, as presented in Sec. VI.

It is well known that the structure of the frequency distribution of emitted radiation is very sensitive to even a small change of emission angles (cf. Fig. 6). Therefore, the question arises: How sensitive is the temporal power distribution of emitted radiation to such a change? To investigate this problem, we shall consider, as above, the emission in the scattering plane. The synthesis of the energy spectrum shown in Fig. 6 leads to the temporal power distribution presented as the color map in Fig. 11. We observe that radiation is emitted in the form of sharp stripes and that, even after integrating with respect to $\Theta_{\boldsymbol{K}}$, the main temporal peaks from Fig. 8 show up for the same ϕ_r. Note that this happens with a smaller contrast, as presented in the upper frame of Fig. 12. In the lower frame of Fig. 12, we also depict the partially integrated energy distribution, given by Eqs. (29) and (40). It shows that, as expected, the high-frequency radiation is emitted in a very narrow cone.

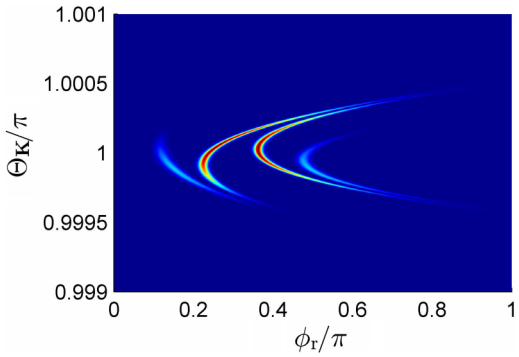

FIG. 11. (Color online) Color map of the power distribution, given by Eq. (38), for the same geometry and parameters as in Fig. 6 and for $\omega_0 = m_e c^2$.

This explains why the very sharp temporal structure survives the integration over the emission angles.

A deeper insight into the coherent properties of the supercontinuum investigated in this paper can be gained by analyzing the phase of the Thomson amplitude, $\mathcal{A}_{\mathrm{Th},\sigma}(\omega_{\boldsymbol{K}})$. By inspecting Figs. 4 and 5, we find that for the laser pulse considered here, the real functions $\Upsilon_\sigma(\phi)$ and $\ell(\phi)$ satisfy the following symmetry relations:

$$\Upsilon_\sigma(\phi) = -\Upsilon_\sigma(2\pi - \phi), \tag{43}$$

and

$$\ell(\phi) + \ell(2\pi - \phi) = 2\ell(\pi). \tag{44}$$

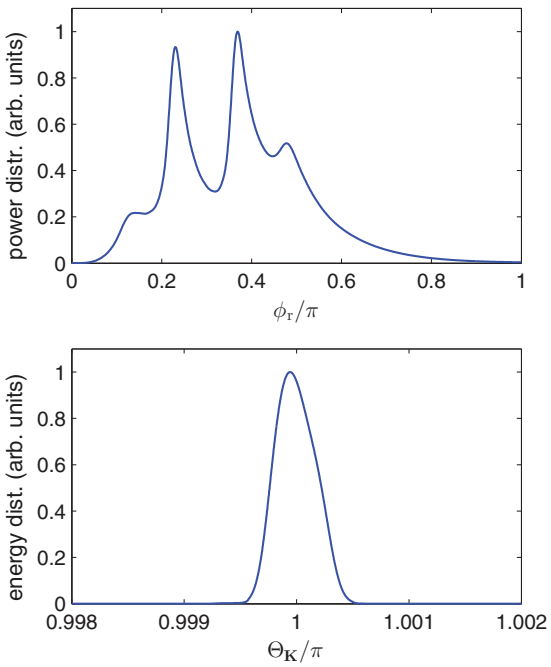

FIG. 12. (Color online) Upper panel: Integrated over $\Theta_{\boldsymbol{K}}$ power distribution, given by Eq. (39), as a function of the retarded phase ϕ_r for $\omega_0 = m_e c^2$. Lower panel: the integrated energy distribution, given by Eqs. (29) and (40), as a function of $\Theta_{\boldsymbol{K}}$ for $\Phi_{\boldsymbol{K}} = \pi/2$. Both distributions are normalized to their maximum values, and the remaining parameters are the same as in Figs. 6 and 11.

These relations allow us to write the Thomson amplitude in the form

$$\mathcal{A}_{\mathrm{Th},\sigma}(\omega_{\boldsymbol{K}}) = \frac{1}{\pi} e^{i\Phi_{\mathrm{Th}}(\omega_{\boldsymbol{K}})} \int_0^\pi d\phi \Upsilon_\sigma(\phi) \times \sin\left\{\frac{\omega_{\boldsymbol{K}}}{c}[\ell(\phi) - \ell(\pi)]\right\}, \tag{45}$$

where the Thomson phase $\Phi_{\mathrm{Th}}(\omega_{\boldsymbol{K}})$,

$$\Phi_{\mathrm{Th}}(\omega_{\boldsymbol{K}}) = \arg \mathcal{A}_{\mathrm{Th},\sigma}(\omega_{\boldsymbol{K}}) = \pm\frac{\pi}{2} + \frac{\ell(\pi)}{c}\omega_{\boldsymbol{K}}, \tag{46}$$

is linear in $\omega_{\boldsymbol{K}}$. Here, "+" corresponds to the case when the last integral in (45) is positive, whereas "−" relates to the case when it is negative. In either case, the constant term does not play a physical role, whereas the linear term *only* introduces an extra time delay, $\ell(\pi)/c$, for the arrival of the generated radiation to a detector. This time delay increases with increasing the intensity of the laser pulse, but does not modify the temporal shape of the emitted radiation. Moreover, for $\Theta_{\boldsymbol{K}}$ close to π, we find the following expression, exact up to the quadratic term in $\Theta_{\boldsymbol{K}} - \pi$:

$$\ell(\pi) = \frac{c\pi}{\omega} + 2z(\pi) + \frac{x^2(\pi)}{2z(\pi)} - \frac{1}{2}z(\pi)\left[\Theta_{\boldsymbol{K}} - \pi - \frac{x(\pi)}{z(\pi)}\right]^2. \tag{47}$$

This explains qualitatively well the parabolic shape of stripes presented in Fig. 11 [for the laser- and electron-beam parameters considered, $x(\pi) \approx 97\lambda\!\!\!^{-}_{\mathrm{C}}$ and $z(\pi) \approx -0.16 \times 10^7 \lambda\!\!\!^{-}_{\mathrm{C}}$].

It is important to note that synthesis of the Thomson energy distribution into a sequence of well-separated and ultrashort pulses of generated radiation is only possible if the phase of the Thomson amplitude is well approximated by the linear dependence on the frequency of emitted radiation. In fact, any significant deviation from such a rule washes away the ultrashort structure of generated radiation. It appears that the genuine quantum recoil of electrons during the emission of photons generates a nonlinear dependence of phases of the Compton amplitudes $\mathcal{A}_{\mathrm{C},\sigma}(\omega_{\boldsymbol{K}}, \lambda_{\mathrm{i}}, \lambda_{\mathrm{f}})$ [see Eq. (9)] on $\omega_{\boldsymbol{K}}$ and, hence, it can lead to the disappearance of ultrashort temporal structures of emitted radiation.

VI. ULTRASHORT-PULSE GENERATION—THOMSON VERSUS COMPTON PROCESSES

We note that the Thomson process can only be considered as an approximation of the fundamental Compton scattering, which describes the actual physical situation with the electron spin degrees of freedom and its recoil included. Therefore, it is important to analyze not only similarities but also differences between these two approaches. These problems have been studied in Ref. [20] in the context of the frequency scaling law. The aim of this section is to discuss discrepancies between the predictions of these two approaches for the generation of very short pulses of emitted radiation.

A great advantage of the classical approach is that calculations can be easily performed even for arbitrary space- and time-dependent laser fields. For this reason, it is extensively used in plasma physics and also in the context of ultrashort-pulse generation [27–32]. However, Thomson theory has some

important shortcomings. For instance, it does not account for the spin of electrons, which for the high-frequency part of the spectrum becomes important [19,20], especially if the spectrum is generated by very short and intense laser pulses. Another defect of the classical theory, which appears to be very crucial for the extremely short-pulse generation, is that it neglects the recoil of electrons during the emission of high-frequency photons [59]. On the other hand, the quantum approach, based on strong-field quantum electrodynamics (QED), accounts for the spin and recoil effects, but the calculations for arbitrary space- and time-dependent laser fields are at the moment not possible. The reason is that the exact solutions of the Dirac equation for such laser pulses are not known. In fact, the pioneering analyses of fundamental QED processes in strong laser fields were limited to monochromatic infinite plane waves [60–62] or to pulses with slowly changing envelopes [10]. However, starting with the seminal paper by Boca and Florescu [11], precise calculations of Compton scattering became possible for arbitrary short and intense plane-wave-fronted laser pulses [9]. Although still computationally demanding, such investigations allow for a reliable comparison of predictions of quantum and classical approaches for temporarily shaped laser pulses. Note that such pulses very well describe the interaction with sufficiently energetic electron beams, provided that the kinetic energy of electrons is much larger than their ponderomotive energy in the laser field (see, e.g., [63,64]).

As it was noted by Sarachik and Schappert [59], the electron recoil effects are small if

$$\omega_{\boldsymbol{K}} \ll \omega_{\rm cut} = c\frac{n\cdot p_{\rm i}}{n\cdot n_{\boldsymbol{K}}}, \tag{48}$$

which does not depend explicitly on either the laser-field intensity (measured by the dimensionless parameter μ) or the laser-field carrier frequency, $\omega_{\rm L}$. Note that for small μ, only the low-frequency part of the emitted spectrum is generated with a significant probability and, therefore, the condition above is typically satisfied. Hence, the inequality (48) can be interpreted as the one which implicitly puts bounds for intense laser fields when the emission of photons from the high-frequency spectrum (of $\omega_{\boldsymbol{K}}$ that is smaller but comparable to $\omega_{\rm cut}$) takes place with significant probabilities. In this sense, the applicability condition (48) is important for the laser-field parameters considered in Sec. III, where the coincidence between the quantum and classical theory has been clearly demonstrated only for the low-frequency part of the spectrum. On the other hand, for smaller laser-field intensities investigated in Secs. IV and V, this condition can be considered as carrying no information since the high-frequency part of the spectrum is generated with marginal probabilities anyway. Sometimes another applicability condition for the classical theory is formulated as an inequality,

$$\mu\omega_{\rm L}\frac{n\cdot p_{\rm i}}{m_e^2c^3} \ll 1, \tag{49}$$

in which the laser-field intensity and the laser carrier frequency appear. This condition is also very well satisfied by parameters considered in Secs. IV and V.

It follows from the Fourier analysis that broader energy spectra have to be used in order to synthesize shorter radiation pulses. There are two possibilities to increase the bandwidth of the energy distribution in Thomson or Compton processes. Namely, one can either increase the energy of a colliding electron beam or increase the intensity of a driving laser beam. Mostly, the second scenario is used [27,29–32]. In this context, we consider the same particle and laser-beam parameters as in Fig. 8, but for $\mu = 10$, which for the Ti:sapphire laser field of the wavelength 800 nm corresponds to the intensity of the order of 10^{20} W/cm^2. The upper panel in Fig. 13 presents the energy distribution calculated from the classical Thomson theory. As anticipated, the energy bandwidth is now 10 times broader as compared to the case of $\mu = 1$. As it was mentioned above, for larger laser-field intensities, the pulses are more delayed in time as compared to lower intensities, but their structure remains the same; it consists of two main central half pulses and two smaller side pulses, as in Fig. 8. All of these pulses are now 10 times shorter, which means that they last for around 10 yoctoseconds. This is demonstrated for one of the main peaks in the lower panel of Fig. 13. The question arises: Is this picture real? In order to answer this question, let us remark that, for the considered geometry and electron energies, the cutoff frequency $\omega_{\rm cut}$ is around $1000m_ec^2$, which is equal to the bandwidth of the energy spectrum used for the synthesis of such short radiation pulses. In the actual physical situation, which is described by the quantum Compton theory, such frequencies cannot be achieved due to the electron recoil. Indeed, the corresponding calculation for Compton scattering shows that the energy distribution is now twice as narrow, as presented in the upper panel of Fig. 14. However, this does not mean that the emitted

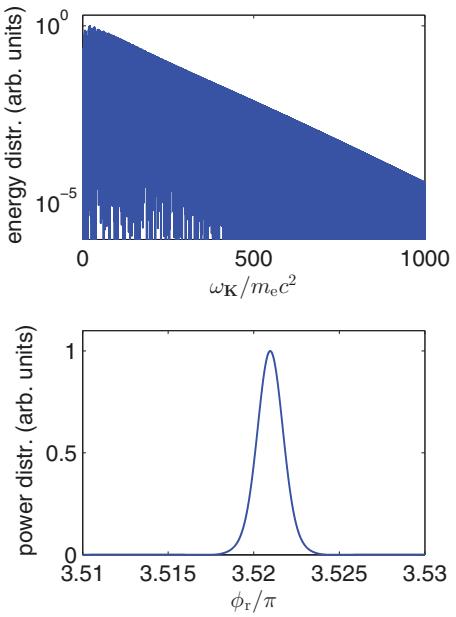

FIG. 13. (Color online) The same as in Fig. 8, but for $\mu = 10$. The energy distribution of emitted radiation extends now to larger frequencies. The synthesis of this energy spectrum leads to the temporal power distribution of emitted radiation similar to the one presented in the lower frame in Fig. 8, except that now individual peaks are approximately ten times narrower. For this reason, only one of the two main peaks is shown in the lower frame.

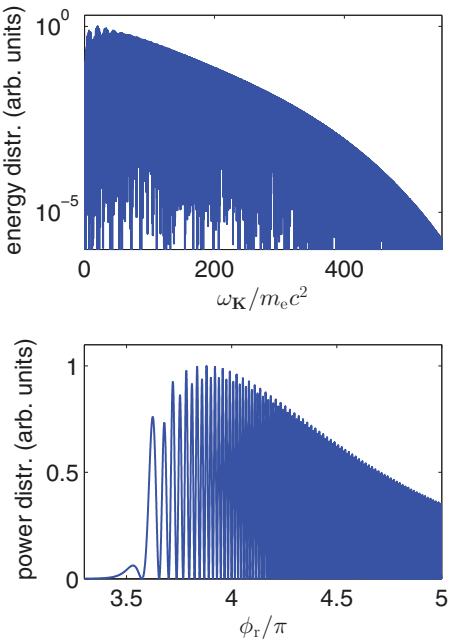

FIG. 14. (Color online) The same as in Fig. 13, but for the quantum Compton process with the electron spin conserved, $\lambda_i\lambda_f = 1$. In contrast to classical results, now the energy distribution extends to smaller frequencies and the synthesized temporal power distribution becomes much broader.

pulses are two times longer. The reason being that, except for squeezing in the frequency domain, the phase of the Compton amplitude depends nonlinearly on the frequency of emitted photons, which we have checked numerically. Even though the condition (49) is quite well satisfied for the parameters of laser and electron beams considered in Figs. 13 and 14, we observe a significant difference between pulses synthesized from classical (Fig. 13) and quantum (Fig. 14) radiation. It follows from classical theory that for the driving pulses considered in this paper, the global phase of the scattering amplitude depends linearly on $\omega_{\boldsymbol{K}}$. As explained in Sec. V, this leads only to a time delay of the generated ultrashort pulses of radiation. On the other hand, in the quantum case, the global phase of scattering amplitude has significant nonlinear dependence on $\omega_{\boldsymbol{K}}$. This prevents the coherent synthesis of the frequency spectrum into very short pulses, as illustrated in the lower panel of Fig. 14. In order to avoid this problem, one has to increase the electron-beam energy, while increasing the laser-field intensity as well.

VII. CONCLUSIONS

An appearance of a broad bandwidth radiation (spanning a few MeV), which is sharply elongated around the propagation direction of the electron beam, has been demonstrated from nonlinear Thomson (Compton) scattering. Our analysis of temporal distributions of the observed radiation shows that it can be used for the synthesis of zeptosecond (likely even yoctosecond) pulses. Note that this is possible provided that the broad bandwidth radiation is coherent, which clearly proves that nonlinear Thomson or Compton scattering can lead to a generation of a supercontinuum.

When analyzing properties of the formed zeptosecond pulses, we discovered that these are one-cycle (half-cycle) pulses. We have also seen that Thomson (Compton) radiation is very sensitive to a change of its emission direction. However, as we showed in this paper, the ultrashort pulses survive the space averaging. In light of this fact, we conclude that the Thomson (Compton) process can be used as a source of zeptosecond (yoctosecond) pulsed radiation. This, in further perspective, will enable the entrance to new physical regimes of intense laser physics.

Additionally, we demonstrated an important role of the global phase for the synthesis of ultrashort-pulse generation. Specifically, we showed that the global phase of the Thomson probability amplitude is a linear function of the energy of emitted radiation, $\omega_{\boldsymbol{K}}$. This guarantees that emitted radiation is coherent and can be synthesized into ultrashort pulses, which is in line with previously published papers [27–32]. We also demonstrated that increasing the driving field intensity does not lead to the synthesis of shorter pulses of radiation. Once the intensity is increased, an electron recoil becomes important. In this case, which can be accounted for only by the Compton theory, the global phase of scattering probability amplitude becomes a nonlinear function of $\omega_{\boldsymbol{K}}$. This results in the broadening of temporal characteristics of produced radiation. While the classical calculations always result in very short pulses of radiation with symmetric temporal profiles (see Fig. 13 and Refs. [27–32]), the actual physical situation is different, as described by means of quantum theory (see Fig. 14). This proves the crucial role played by the global phase of Thomson and Compton amplitudes in the synthesis of short radiation pulses.

ACKNOWLEDGMENT

This work is supported by the Polish National Science Center (NCN) under Grant No. 2012/05/B/ST2/02547.

[1] T. Tajima and J. M. Dawson, Phys. Rev. Lett. **43**, 267 (1979).
[2] K. Ta Phuoc, S. Corde, C. Thaury, V. Malka, A. Tafzi, J. P. Goddet, R. C. Shah, S. Sebban, and A. Rousse, Nat. Photon. **6**, 308 (2012).
[3] S. Corde, K. Ta Phuoc, G. Lambert, R. Fitour, V. Malka, A. Rousse, A. Beck, and E. Lefebvre, Rev. Mod. Phys. **85**, 1 (2013).
[4] D. Umstadter, J. Phys. D: Appl. Phys. **36**, R151 (2003).
[5] Y. Y. Lau, F. He, D. P. Umstadter, and R. Kowalczyk, Phys. Plasmas **10**, 2155 (2003).
[6] F. Ehlotzky, K. Krajewska, and J. Z. Kamiński, Rep. Prog. Phys. **72**, 046401 (2009).
[7] A. Di Piazza, C. Müller, K. Z. Hatsagortsyan, and C. H. Keitel, Rev. Mod. Phys. **84**, 1177 (2012).
[8] http://www.extreme-light-infrastructure.eu
[9] R. A. Neville and F. Rohrlich, Phys. Rev. D **3**, 1692 (1971).
[10] N. B. Narozhny and M. S. Fofanov, JETP **83**, 14 (1996).
[11] M. Boca and V. Florescu, Phys. Rev. A **80**, 053403 (2009).

[12] F. Mackenroth, A. Di Piazza, and C. H. Keitel, Phys. Rev. Lett. **105**, 063903 (2010).
[13] F. Mackenroth and A. Di Piazza, Phys. Rev. A **83**, 032106 (2011).
[14] D. Seipt and B. Kämpfer, Phys. Rev. A **83**, 022101 (2011).
[15] M. Boca and V. Florescu, Eur. Phys. J. D **61**, 449 (2011).
[16] M. Boca, V. Dinu, and V. Florescu, Phys. Rev. A **86**, 013414 (2012).
[17] K. Krajewska and J. Z. Kamiński, Phys. Rev. A **85**, 062102 (2012).
[18] F. Mackenroth and A. Di Piazza, Phys. Rev. Lett. **110**, 070402 (2013).
[19] K. Krajewska and J. Z. Kamiński, Laser Part. Beams **31**, 503 (2013).
[20] K. Krajewska and J. Z. Kamiński, arXiv:1308.1663.
[21] K. Krajewska, C. Müller, and J. Z. Kamiński, Phys. Rev. A **87**, 062107 (2013).
[22] S. P. Roshchupkin, A. A. Lebed', E. A. Padusenko, and A. I. Voroshilo, Laser Phys. **22**, 1113 (2012).
[23] S. P. Roshchupkin, A. A. Lebed', and E. A. Padusenko, Laser Phys. **22**, 1513 (2012).
[24] M. Boca, Cent. Eur. J. Phys. **11**, 1123 (2013).
[25] A. A. Lebed' and S. P. Roshchupkin, Laser Phys. **23**, 125301 (2013).
[26] I. Ghebregziabher, B. A. Shadwick, and D. Umstadter, Phys. Rev. ST Accel. Beams **16**, 030705 (2013).
[27] A. L. Galkin, V. V. Korobkin, M. Yu. Romanovsky, and O. B. Shiryaev, Contrib. Plasma Phys. **49**, 593 (2009).
[28] S.-Y. Chung, M. Yoon, and D. E. Kim, Opt. Express **17**, 7853 (2009).
[29] K. Lee, Y. H. Cha, M. S. Shin, B. H. Kim, and D. Kim, Phys. Rev. E **67**, 026502 (2003).
[30] P. Lan, P. Lu, W. Cao, and X. Wang, Phys. Rev. E **72**, 066501 (2005).
[31] A. E. Kaplan and P. L. Shkolnikov, Phys. Rev. Lett. **88**, 074801 (2002).
[32] F. Liu and O. Willi, Phys. Rev. ST Accel. Beams **15**, 070702 (2012).
[33] K. Zhao, Q. Zhang, M. Chini, Y. Wu, X. Wang, and Z. Chang, Opt. Lett. **37**, 3891 (2012).
[34] M. Ferray, A. L'Huillier, X. F. Li, L. A. Lompré, G. Mainfray, and C. Manus, J. Phys. B **21**, L31 (1988).
[35] A. McPherson, G. Gibson, H. Jara, U. Johann, T. S. Luk, I. A. McIntyre *et al.*, J. Opt. Soc. Am. B **4**, 595 (1987).
[36] Gy. Farkas and Cs. Tóth, Phys. Lett. A **168**, 447 (1992).
[37] M. C. Köhler, T. Pfeifer, K. Z. Hatsagortsyan, and C. H. Keitel, Adv. At. Mol. Opt. Phys. **61**, 159 (2012).
[38] B. Shan and Z. Chang, Phys. Rev. A **65**, 011804(R) (2001).
[39] C. Hernández-García, J. A. Pérez-Hernández, T. Popmintchev, M. M. Murnane, H. C. Kapteyn, A. Jaroń-Becker, A. Becker, and L. Plaja, Phys. Rev. Lett. **111**, 033002 (2013).
[40] B. W. J. McNeil and N. R. Thompson, Nat. Photon. **4**, 814 (2010).
[41] D. J. Dunning, B. W. J. McNeil, and N. R. Thompson, Phys. Rev. Lett. **110**, 104801 (2013).
[42] J. D. Jackson, *Classical Electrodynamics* (Wiley, New York, 1975).
[43] L. D. Landau and E. M. Lifshitz, *The Classical Theory of Field* (Butterworth-Heinemann, Oxford, 1987).
[44] Y. I. Salamin and F. H. M. Faisal, Phys. Rev. A **54**, 4383 (1996).
[45] F. V. Hartemann and A. K. Kerman, Phys. Rev. Lett. **76**, 624 (1996).
[46] F. V. Hartemann, *High-Field Electrodynamics* (CRC, Boca Raton, FL, 2002).
[47] K. Krajewska and J. Z. Kamiński, Phys. Rev. A **86**, 021402(R) (2012).
[48] R. R. Alfano and S. L. Shapiro, Phys. Rev. Lett. **24**, 584 (1970); **24**, 592 (1970).
[49] J. M. Dudley, G. Genty, and S. Coen, Rev. Mod. Phys. **78**, 1135 (2006).
[50] B. R. Washburn, S. A. Diddams, N. R. Newbury, J. W. Nicholson, M. F. Yan, and C. G. Jørgensen, Opt. Lett. **29**, 250 (2004).
[51] W. Drexler, U. Morgner, F. X. Kärtner, C. Pitris, S. A. Boppart, X. D. Li, E. P. Ippen, and J. G. Fujimoto, Opt. Lett. **24**, 1221 (1999).
[52] R. T. Neal, M. D. C. Charlton, G. J. Parker, C. E. Finlayson, M. C. Netti, and J. J. Baumberg, Appl. Phys. Lett. **83**, 4598 (2003).
[53] G. Brambilla, F. Koizumi, V. Finazzi, and D. J. Richardson, Electron. Lett. **41**, 795 (2005).
[54] K. Krajewska and J. Z. Kamiński, Phys. Rev. A **86**, 052104 (2012).
[55] K. Krajewska and J. Z. Kamiński, Laser Phys. Lett. **11**, 035301 (2014).
[56] F. Krausz and M. Ivanov, Rev. Mod. Phys. **81**, 163 (2009).
[57] R. A. Ganeev, Laser Phys. Lett. **9**, 175 (2012).
[58] F. H. M. Faisal and J. Z. Kamiński, Phys. Rev. A **54**, R1769 (1996).
[59] E. S. Sarachik and G. T. Schappert, Phys. Rev. D **1**, 2738 (1970).
[60] V. I. Ritus and A. I. Nikishov, *Quantum Electrodynamics of Phenomena in Intense Fields*, Trudy FIAN SSSR Vol. 111 (Nauka, Moscow, 1979).
[61] L. S. Brown and T. W. B. Kibble, Phys. Rev. **133**, A705 (1964).
[62] T. W. B. Kibble, Phys. Rev. **138**, B740 (1965).
[63] M. Twardy, K. Krajewska, and J. Z. Kamiński, arXiv:1311.5374 [J. Phys.: Conf. Ser. (to be published)].
[64] K. Lee, S. Y. Chung, S. H. Park, Y. U. Jeong, and D. Kim, Europhys. Lett. **89**, 64006 (2010).